Materials Science & Engineering A xxx (xxxx) xxx

Contents lists available at ScienceDirect

Materials Science & Engineering A

journal homepage: http://www.elsevier.com/locate/msea

# Mechanism of crack initiation and early growth of high strength steels in very high cycle fatigue regime

Qingyuan Song [a,b], Chengqi Sun [a,b,*]

[a] State Key Laboratory of Nonlinear Mechanics, Institute of Mechanics, Chinese Academy of Sciences, Beijing, 100190, China
[b] School of Engineering Science, University of Chinese Academy of Sciences, Beijing, 100049, China

ARTICLE INFO

*Keywords:*
very high cycle fatigue
High strength steels
Crack initiation mechanism
Crack growth rate
Grain refinement

ABSTRACT

In this paper, we capture the evolution characteristic of interior crack initiation and early growth of a bearing steel (GCr15) with tensile strength bigger than 2000 MPa in very high cycle fatigue (VHCF) regime by variable amplitude loadings. The traces left on the fracture surface suggest that the equivalent crack growth rate in crack initiation and early growth stage is of the magnitude $10^{-12}$-$10^{-11}$ m/cyc. Transmission electron microscopy (TEM) observation further shows that there are discontinuous refined grain regions beneath the fracture surface in the crack initiation and early growth region. Moreover, the compressive fatigue test is performed on the specimen of a martensitic stainless steel (AISI630) with a pre-crack, and no grain refinement phenomenon is observed in the vicinity of the crack tip and beneath the crack surface by the electron backscatter diffraction (EBSD). The present results support the mechanism of the crack initiation and early growth of high strength steels in VHCF regime: the crack initiation and early growth is attributed to the grain refinement caused by the dislocation interaction over a number of cyclic loadings followed by micro cracks along with the formation of micro cracks irrespective of the grain refinement during the cyclic loading.

## 1. Introduction

Very high cycle fatigue (VHCF) (fatigue failure beyond $10^7$ loading cycles) has become a new field of fatigue research due to the urgent demand of ultra-long life in safe service [1–6]. For high strength steels, the fatigue crack usually initiates from the interior of the specimen, and a fish-eye pattern with fine granular area (FGA) morphology presents in the vicinity of the crack origin in most cases [7–11], which is quite different from the low cycle fatigue. It has been shown that the FGA consumes more than 90% of the fatigue life [12–14] and that the stress intensity factor range of FGA is almost a constant close to the threshold value of crack propagation $\Delta K_{th}$ [15–17]. Hence, the formation of FGA plays a crucial role in understanding the crack initiation and early growth of high strength steels in VHCF failure.

It has been shown that the microstructure beneath FGA could be a thin layer of nano-grains [18–21], a discontinuous gradient layer composed of coarse and refined grains [22], and no refined grain feature [23]. Moreover, the results by Hong et al. [19] and Kovacs et al. [24] showed that the grain refinement presented at negative stress ratios and no grain refinement was found at positive stress ratios. The existing models for the formation of FGA, such as the "hydrogen assisted crack growth" model [4,25], "decohesion of spherical carbide" model [12], "polygonization and micro-debonding" model [23], "local grain refinement at the crack tip" model [18] and "numerous cyclic pressing" model [19,26], could not explain well all the observed experimental results [22,27]. Further, there is the fact that the fracture surfaces of some high strength steels present no FGA morphology surrounding the crack origin for the fish-eye mode failure in VHCF regime [28,29]. Therefore, it is very essential to explore the mechanism of crack initiation and early growth not only for the formation of FGA in VHCF regime.

The interior crack initiation and very small size of FGA (usually about 10–80 μm [15,17]) make the direct observation very difficult to explore the evolution process of the early crack. Recently, Sun et al. [22,30] captured the evolution characteristic of FGA for a martensitic stainless steel (AISI630) in VHCF regime by using the repeated two-step fatigue test, and estimated the equivalent crack growth rate in FGA by the "tree ring" patterns left on the fracture surface.

In this work, the specially designed variable amplitude loadings are performed on the specimens of a bearing steel GCr15 (a type of high strength steel widely investigated in VHCF regime) with the tensile strength bigger than 2000 MPa, and the compressive fatigue test is carried out for the specimen of a martensitic stainless steel (AISI630)

* Corresponding author. State Key Laboratory of Nonlinear Mechanics, Institute of Mechanics, Chinese Academy of Sciences, Beijing, 100190, China.
*E-mail address:* scq@lnm.imech.ac.cn (C. Sun).

https://doi.org/10.1016/j.msea.2019.138648
Received 8 August 2019; Received in revised form 6 November 2019; Accepted 6 November 2019
Available online 7 November 2019

with a pre-crack. The aim of the paper is to explore the mechanism of the crack initiation and early growth in VHCF regime. Based on the observations by the scanning electron microscopy (SEM), transmission electron microscopy (TEM) and electron backscatter diffraction (EBSD), the mechanism of the crack initiation and early growth is developed for the high strength steels in VHCF regime.

## 2. Materials and methods

### 2.1. Materials

Two materials are used in this paper. One is a high carbon chromium bearing steel GCr15. The chemical compositions are 1.0 C, 1.52 Cr, 0.31 Mn, 0.21 Si, 0.016 S and 0.0086 P in weight percent (Fe balance). The other is a martensitic stainless steel 0cr17ni4cu4nb (AISI630). The chemical compositions (wt.%) are 0.047C, 15.58 Cr, 3.65 Ni, 3.11 Cu, 0.74 Mn, 0.18 Nb, 0.16 Mo and Fe balance. For the bearing steel, the machined specimens are at first heated for 1 h at 850 °C in vacuum furnace. Then, they are oil-quenched and tempered for 2 h at 200 °C in air. The tensile strength of the bearing steel is 2375 MPa. For the stainless steel, the specimens are at first heated for 1 h at 1050 °C and cooled in air. Then, they are heated for 3 h at 850 °C and oil-quenched. Finally, they are tempered for 4 h at 470 °C in air. The tensile strength of the stainless steel is 1161 MPa. The microstructures of the bearing steel and the stainless steel are shown in Fig. 1a and b, respectively.

### 2.2. Fatigue tests

For the bearing steel, two loading sequences are adopted for the fatigue test. One is the constant stress amplitude fatigue test, and the other is the variable (two-step) stress amplitude fatigue test. Both the fatigue tests are performed on a Shimadzu USF-2000 machine ($f$=20 kHz) with stress ratio $R$=−1 in air and at room temperature. The fatigue loading is without intermittence, and the compressive cool air is used to reduce the temperature raise of the specimens during the fatigue test. The two-step fatigue test starts from a sequence of lower stress amplitude $\sigma_{a,L}$=800 MPa with the associated cycles $n_L$=$2\times10^6$ or $3\times10^6$, and then is followed by a sequence of higher stress amplitude $\sigma_{a,H}$ =1100 MPa with the associated cycles $n_H$=$6\times10^3$. This loading sequence is repeated until the failure of the specimen occurs or the total loading cycles of $5\times10^8$ is reached. The specimen geometry for the bearing steel is illustrated in Fig. 2a.

For the stainless steel, an initial crack is at first prefabricated on a notched specimen shown in Fig. 2b by variable stress amplitude fatigue test at the stress ratio $R$=−1. Then, the notch is grounded by grade 1500 abrasive paper, and compressive fatigue test with $5\times10^6$ cyclic loading cycles is performed on the pre-cracked specimen. The maximum stress is 0 MPa and the minimum stress is −430 MPa. The fatigue tests are conducted by the MTS Landmark test system. The frequency is 30 Hz.

Before fatigue test, all the tested surfaces of the specimens are ground and polished in order to eliminate the machining scratches.

### 2.3. Observation and characterization

For the bearing steel specimens, all the fracture surfaces are observed by a scanning electron microscope (SEM) JSM-IT300. By use of the focused ion beam (FIB) technique on the commercial crossbeam 540 FIB-SEM system, several cross-section samples along the loading direction are prepared for the further observation of microstructure beneath the crack initiation and early growth region for the bearing steel specimens, and then observed by the transmission electron microscopy (TEM) with selected area diffraction (SAD) on JEOL 2100F. The diameter of the diffraction area is 170 nm, and a coating layer of platinum is used to protect the fracture surface of the extracted samples during the cutting process. The crack growth lengths due to the variable loading amplitudes are measured from the SEM images by using an Image-Pro Plus (IPP) version 5.0.

For the stainless steel specimen, the electrolytic polishing is carried out after the fatigue test, and then the electron backscatter diffraction (EBSD) technique on the Nordlys of Oxford Instruments is used to observe the microstructure characteristic of the crack tip and the mated crack surfaces.

## 3. Results

### 3.1. Fracture surface for bearing steel specimens

#### 3.1.1. SEM observation of fracture surface under constant amplitude loading

Most of the bearing steel specimens fail from the interior of the specimen and the fracture surfaces present fish-eye patterns under the constant amplitude loading. A few specimens fail from the specimen surface. Fig. 3 shows the fracture surface morphology of several failed specimens with typical fish-eye patterns under different stress amplitudes. It is seen that, for the higher stress amplitude (e.g. $\sigma_a$ =1100 MPa, and $\sigma_a$ =1000 MPa), the FGA hardly forms or there is unclear FGA morphology, as shown in figures A-3 and B-3 in Fig. 3. While for the lower stress amplitude (e.g. $\sigma_a$ =840 MPa), the fracture surface tends to present large and clear FGA, as shown in figure C-3 in Fig. 3.

The S-N data and the FGA size with the stress amplitude under the constant amplitude loading are shown in Fig. 4. It is seen from Fig. 4b that the FGA size tends to increase with the decrease of the stress amplitude. Fig. 4a also indicates that the surface initiated failure mode could occur for the high strength steels in VHCF regime, and the high strength steels could fail at the fatigue life longer than $10^9$ cycles.

#### 3.1.2. SEM observation of fracture surface under variable amplitude loadings

All the seven specimens of the bearing steel under the variable amplitude loadings fail from the interior of the specimen, and present

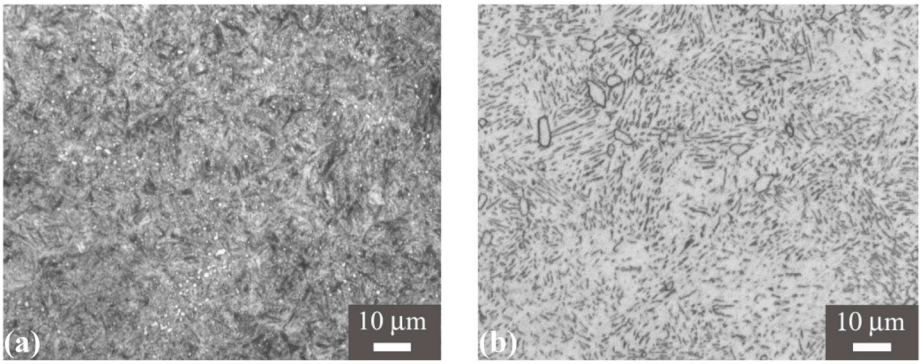


**Fig. 1.** Microstructures of the tested materials. (a) Bearing steel GCr15; (b) Martensitic stainless steel 0cr17ni4cu4nb.

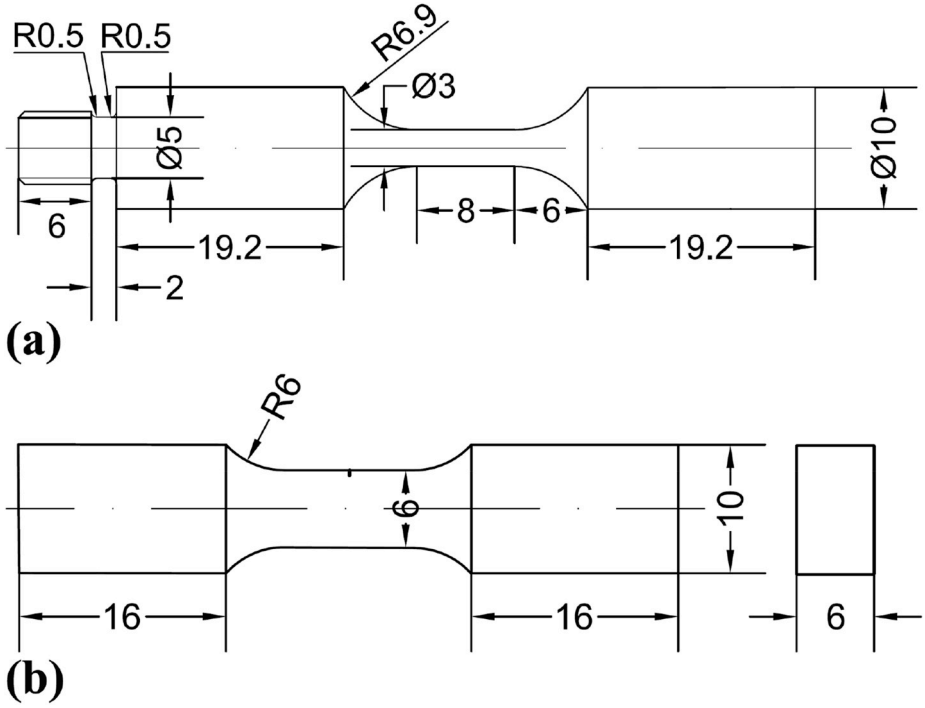


**Fig. 2.** Specimen geometries for fatigue test (in mm). (a) Specimen for bearing steel; (b) Notched specimen for stainless steel with a notch depth of 0.2 mm.

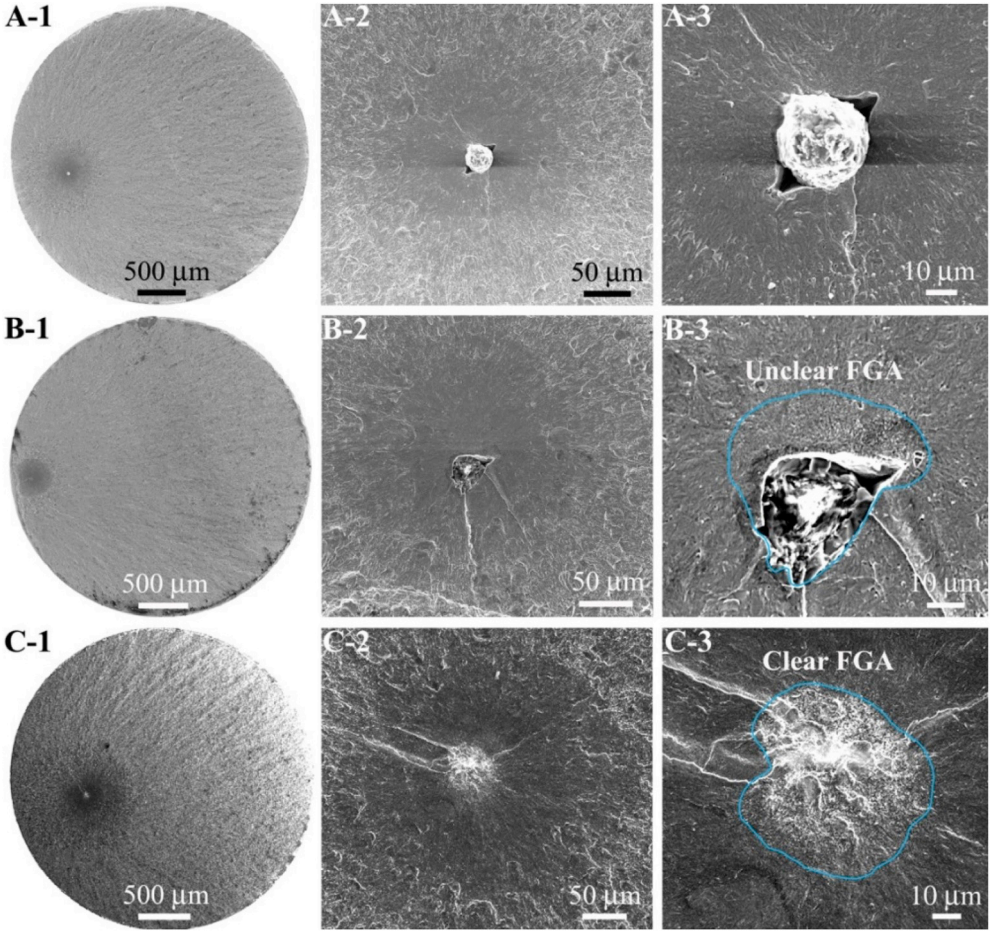


**Fig. 3.** Fracture surface morphology of failed specimens with typical fish-eye patterns under constant amplitude loading. A-1∼A-3: $\sigma_a$=1100 MPa, $N_f$=3.36 × $10^5$; B1-B3: $\sigma_a$=1000 MPa, $N_f$=3.1 × $10^6$; C-1∼C-3: $\sigma_a$=840 MPa, $N_f$=5.90 × $10^8$. A-2, B-2 and C-2 are close-ups of A-1, B-1 and C-1, respectively; A-3, B-3 and C-3 are close-ups of A-2, B-2 and C-2, respectively.

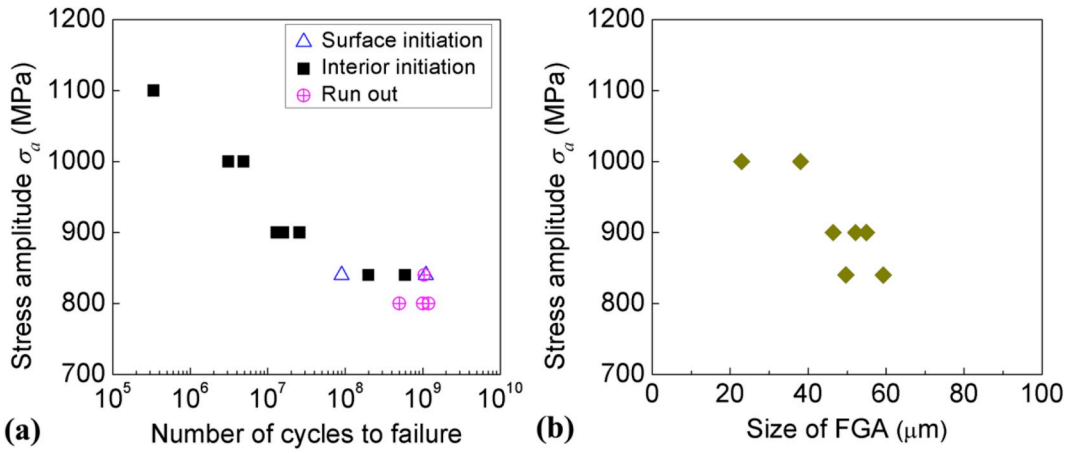


**Fig. 4.** (a) S-N data under constant amplitude loading; (b) Size of FGA versus stress amplitude for interior crack initiation in (a).

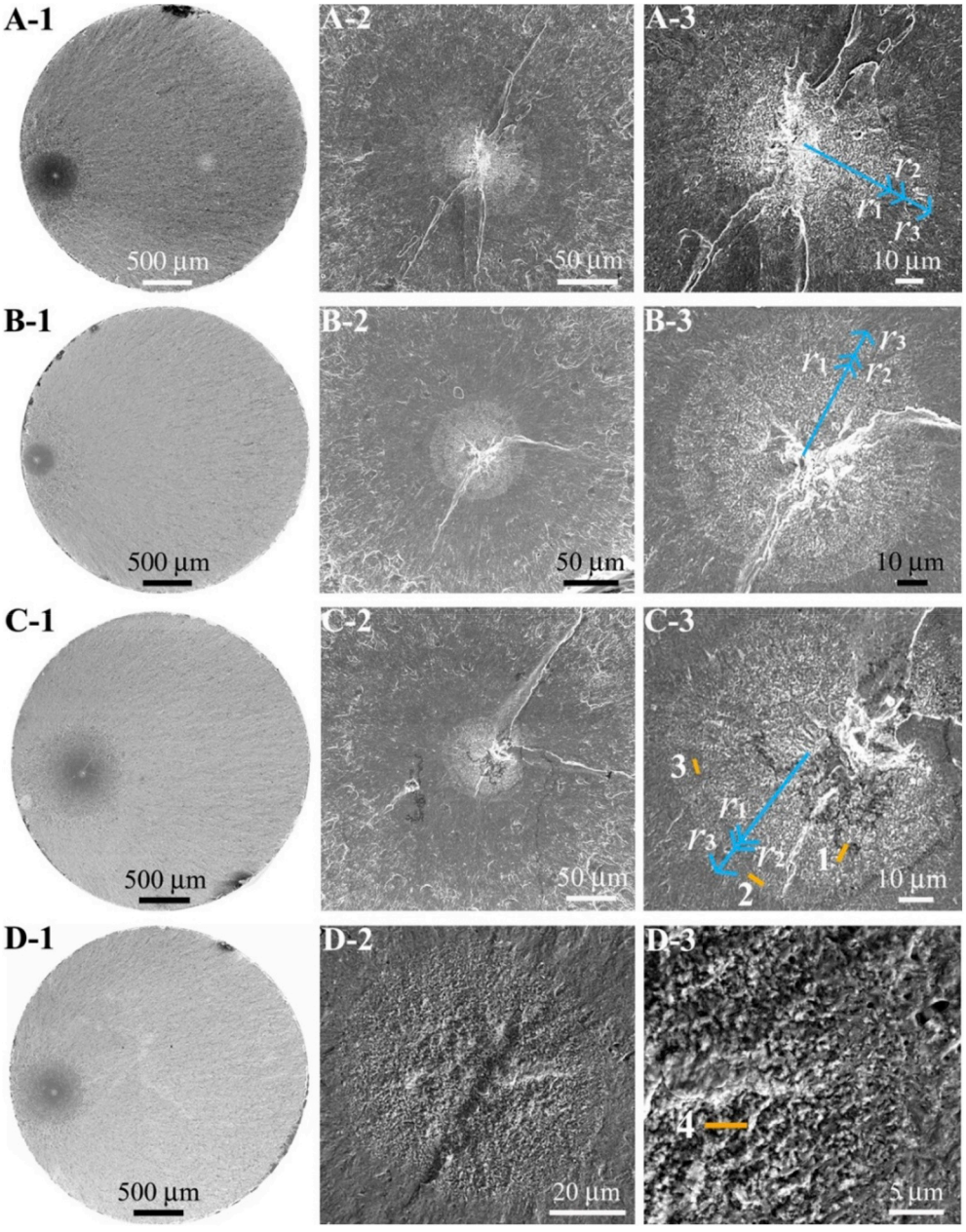


**Fig. 5.** SEM observations of failed specimens with fish-eye like patterns under variable amplitude loadings. A-1~A-3: At a total fatigue life of $1.3674 \times 10^8$ ($n_L$=$2 \times 10^6$, $n_H$ =$6 \times 10^3$); B-1~B-3: At a total fatigue life of $6.1279 \times 10^7$ ($n_L$=$3 \times 10^6$, $n_H$ =$6 \times 10^3$); C-1~C-3: At a total fatigue life of $1.8723 \times 10^8$ ($n_L$=$3 \times 10^6$, $n_H$ =$6 \times 10^3$); D-1~D-3: At a total fatigue life of $1.3041 \times 10^8$ ($n_L$=$3 \times 10^6$, $n_H$ =$6 \times 10^3$); A-2, B-2, C-2 and D-2 are close-ups of A-1, B-1, C-1 and D-1, respectively; A-3, B-3, C-3 and D-3 are close-ups of A-2, B-2, C-2 and D-2, respectively. $r_1$ and $r_3$ in A-3, B-3 and C-3 denote the radius of the crack after the loading sequence of the lower stress amplitude, and $r_2$ denotes the radius of the crack after the loading sequence of the higher stress amplitude. The numbers 1, 2, 3 and 4 in C-3 and D-3 denote the locations of extracted cross-section samples for TEM observation.

fish-eye like patterns as those found under the constant amplitude loading, as shown in Fig. 5. Based on the characteristic of the fracture surface under the constant amplitude loading in Figs. 3 and 4, the relative smooth areas between the rough areas in figures A-3, B-3 and C-3 in Fig. 5 are caused by the higher stress amplitude $\sigma_{a,H}$ =1100 MPa. Moreover, according to the present loading sequence (i.e. the lower stress amplitude $\sigma_{a,L}$ is $2 \times 10^6$ or $3 \times 10^6$ cycles in the repeated two-step loading sequence), the formation of FGA morphology could present for hundreds of thousands of cyclic loadings.

### 3.1.3. TEM observation of crack initiation and early growth region

Four cross-section samples from the fish-eye region of the fracture surface are prepared for the failed specimens under the variable amplitude loadings by FIB technique. The cutting locations are shown in figures C-3 and D-3 in Fig. 5. Samples 1, 2 and 4 are located in the FGA (i.e. the rough area). Sample 3 is located in the smooth area between the rough areas.

The TEM images and SAD diffraction patterns for the extracted cross-section samples 1-4 are shown in Fig. 6a-d, respectively. It is seen that, for samples 1, 2 and 4 in the FGA, the SAD pattern with diffused rings or a lot of tiny spots in locations C, N and P indicates a characteristic of refined grains, while the SAD pattern with isolated spots in locations A and D or discontinuous circles in locations B, F and G suggests just a few grains, the SAD patterns with regular spots in locations E, H, M and O implies just one grain. This indicates that the refined grains only exist in some regions beneath FGA for the bearing steel. This result is the same as that observed for the martensitic stainless steel (AISI630) in VHCF regime [22]. For sample 3 extracted from the smooth area, the common

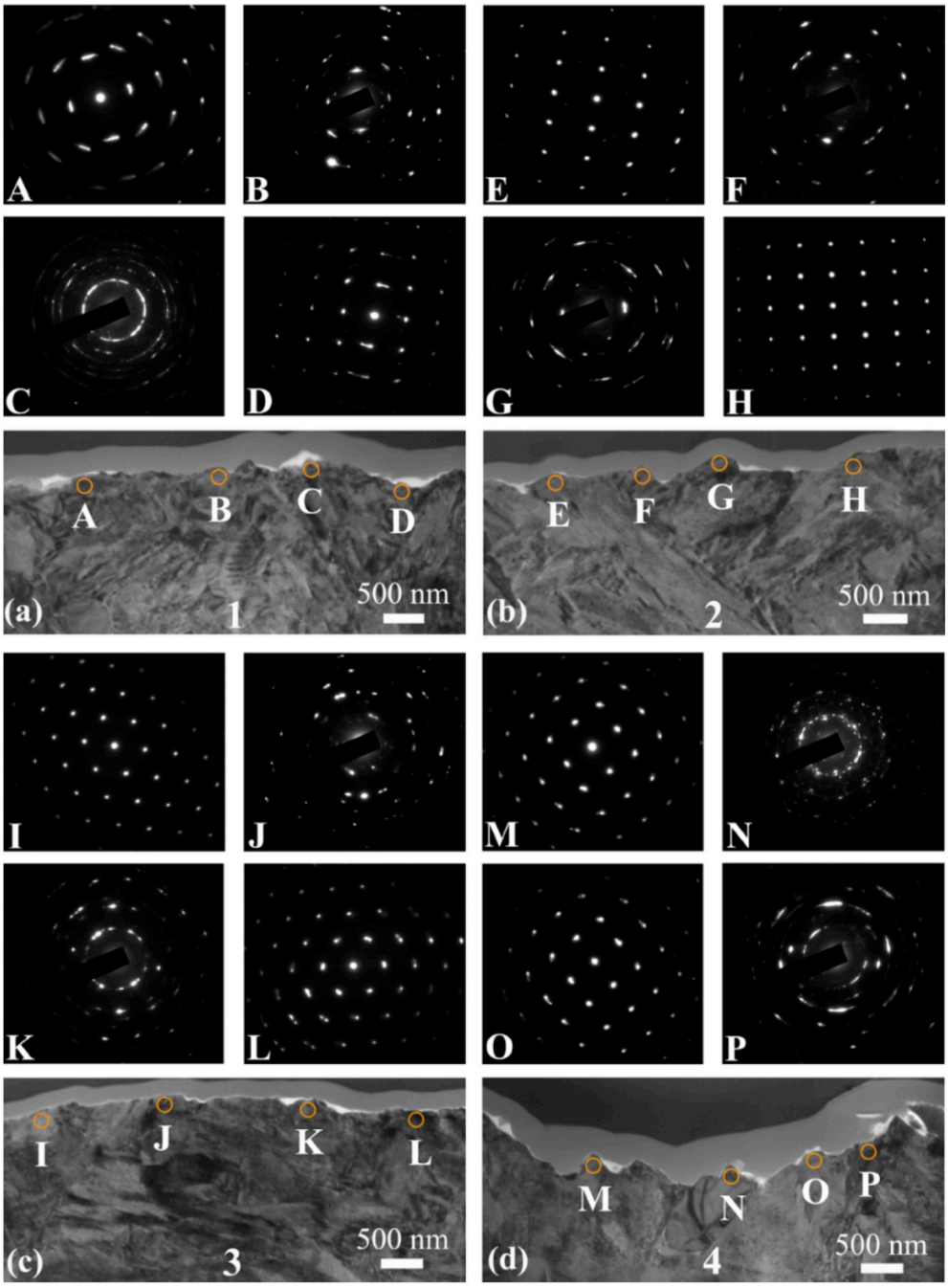


**Fig. 6.** (a)-(d) TEM images and SAD diffraction patterns for the extracted cross-section samples 1-4 in Fig. 5c and d under variable amplitude loadings, respectively, where the circles indicate the locations of the SAD diffraction.

grain feature (location I) and the characteristic of the refined grains (location K) are also observed beneath the fracture surface. This phenomenon might be explained that the refined grains form at first in some local regions due to the loading sequence of the lower stress amplitude and the following sequence of the higher stress amplitude induces the smooth morphology.

### 3.2. EBSD observation of crack tip and mated crack surfaces for stainless steel specimen

The EBSD results of the crack tip and the mated crack surfaces for the pre-cracked specimen under the compressive fatigue test are shown in Fig. 7. The observation region is parallel to the loading direction, including a part of the pre-crack and the region around the pre-crack tip (the initial pre-crack is about 190 μm), as shown in Fig. 7a. The scanning step size is 40 nm for the EBSD images. It is seen from Fig. 7 that there is no grain refinement in the vicinity of the crack tip and the region beneath the crack surface. According to the results by Sun et al. [22] for the same material under the variable stress amplitudes, the number of $5 \times 10^6$ cyclic loadings would be enough to induce the FGA morphology (or grain refinement) for the initiated interior crack at the stress amplitude of 430 MPa and the stress ratio $R=-1$. This indicates that the grain refinement is related to the stress ratio (i.e. the loading condition) [19], and that only a large number of cyclic compressive loadings (the maximum compressive stress is much lower than the yield strength of the material) might not result in the grain refinement at the crack tip or beneath the crack surface.

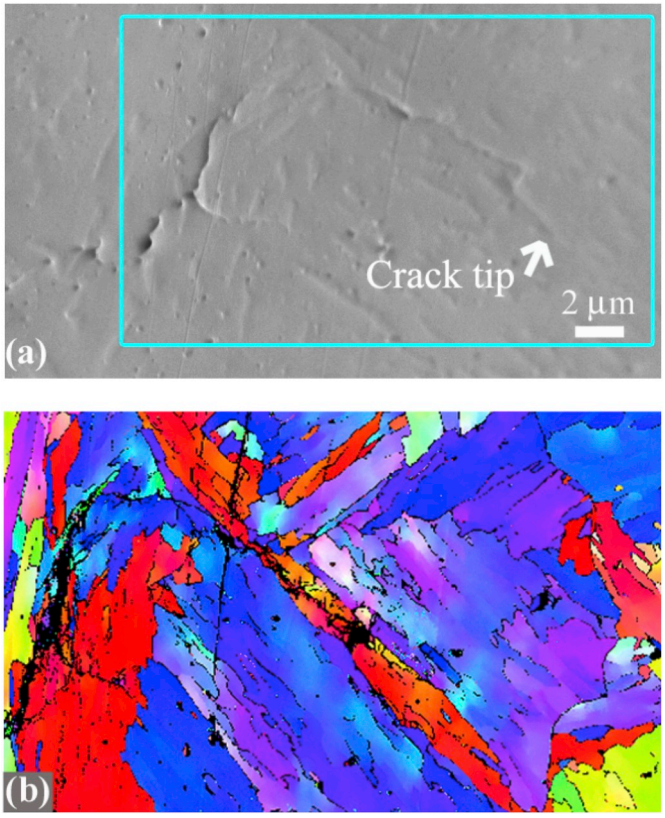


**Fig. 7.** SEM image and EBSD result of the crack tip and the mated crack surfaces for the specimen under compressive fatigue test. (a) SEM image; (b) EBSD inverse pole figure maps for the rectangle region in (a).

## 4. Discussion

### 4.1. Crack growth rate in FGA

Based on the marks left in the fracture surface due to the high and the low stress amplitude associated with the corresponding loading cycles, the crack initiation rate in FGA is estimated. It is assumed that the cracks before and after the loading sequence of the higher stress amplitude could be seen as concentric mode-I internal penny cracks in an infinite solid [30], as shown in Fig. 8a. For a mode-I internal penny crack with radius $a$ in an infinite solid under a uniform remote tensile stress $\sigma$, the stress intensify factor could be expressed as $2\sigma\sqrt{a/\pi}$ [31]. Taking $(r_2-r_1)/2+r_1$ as the radius of the penny crack after the loading sequence of the higher stress amplitude and $(r_3-r_2)/2+r_2$ as the radius of the penny crack after the loading sequence of the lower stress amplitude, the corresponding value of $\Delta K$ is obtained by $\sigma_{a,H}\sqrt{2(r_1+r_2)/\pi}$ for the high stress and by $\sigma_{a,L}\sqrt{2(r_2+r_3)/\pi}$ for the low stress, where $r_1$ and $r_3$ denote the radii of the cracks after the loading sequence of the lower stress amplitude, and $r_2$ denotes the radius of the crack before the loading sequence of the lower stress amplitude, as also shown in figure A-3, B-3 and C-3 in Fig. 5. The associated crack growth rate $\mathrm{d}a/\mathrm{d}N$ is obtained by $(r_2-r_1)/n_H$ for the high stress and by $(r_3-r_2)/n_L$ for the low stress. Here, the stress amplitude is used instead of the stress range for the stress ratio $R=-1$ [8,17].

The relation between the crack growth rate and the value of $\Delta K$ is plotted in Fig. 8b. It is seen that the crack growth rate due to the loading sequence of the higher stress amplitude (i.e. in the smooth area between the rough areas in the fracture surface) is bigger than $10^{-10}$ m/cyc. While the crack growth rate in the rough area is very small and much lower than $10^{-10}$ m/cyc.

### 4.2. Critical size of FGA

On the critical size of FGA, several models have been proposed from the relation between the plastic zone size of the crack tip and the size of microstructural feature [10,16] or the increment of crack length in one stress cycle [32]. From the view of crack propagation, the equivalent crack growth length in FGA is much lower than one lattice spacing ($\sim 10^{-10}$ m) per cycle, i.e. FGA is formed during the process of crack growth rate lower than $10^{-10}$ m/cyc. According to the results by Marines-Garcia et al. [33], at the threshold corner location, $\mathrm{d}a/\mathrm{d}N = b$ and $\Delta K_{\mathrm{eff}} = E\sqrt{b}$, where $E$ is elastic modulus and $b$ is the magnitude of Burger's vector. For high strength steels, the value of $\Delta K_{\mathrm{eff}}$ is about 3.3 MPa $\mathrm{m}^{1/2}$, which might be regarded as the lower bounder of the value of $\Delta K_{\mathrm{FGA}}$ [17]. So, it is thought that the threshold value of the crack propagation $\Delta K_{\mathrm{th}}$ could be regarded as the condition that the formation of FGA is completed. This is also consistent with that the value of $\Delta K_{\mathrm{FGA}}$ is close to $\Delta K_{\mathrm{th}}$.

### 4.3. Mechanism of crack initiation and early growth

The present EBSD results of the crack tip and the mated crack surfaces for the specimen of the martensitic stainless steel with initial pre-crack under the compressive fatigue test indicate that the grain refinement is formed during the crack initiation and evolution process, rather than by a large number of repeating compressive loadings after the fatigue crack initiated. This is consistent with the observation of the refined grains in front of the crack tip for high strength steels [22,27]. It is noted that a general idea is that the vacuum condition is important for the formation of the FGA [10,20]. The present compressive fatigue test is performed in air. According to the results by Tofique et al. [21], the FGA feature and the fine grained layers could be formed on the fracture surface in air for cold rolled stainless steels in VHCF regime. So, the air environment is thought to be no influence on the grain refinement of the tested stainless steel.

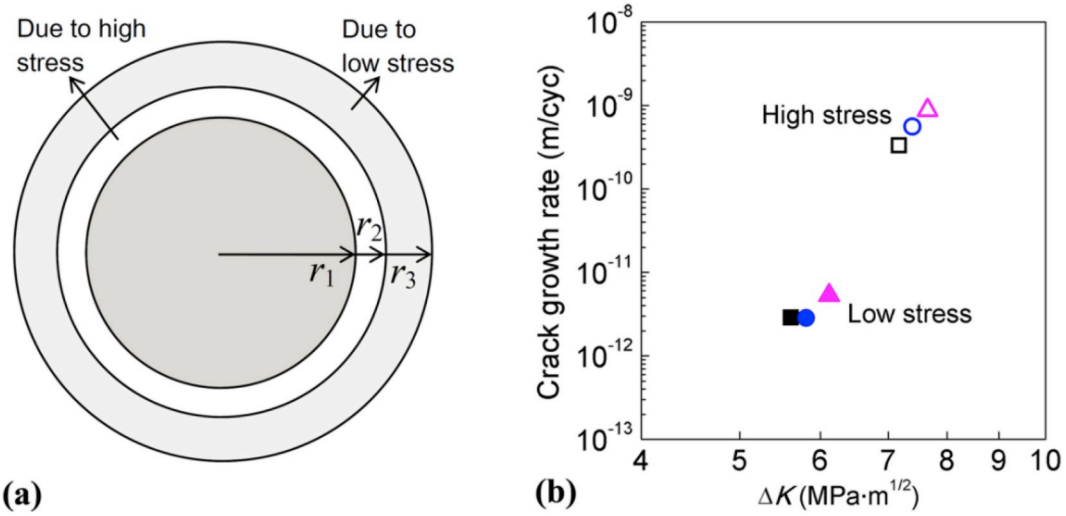


**Fig. 8.** (a) Sketch map of concentric penny cracks under variable amplitude loadings; (b) Crack growth rate with the stress intensity factor range, in which the symbols denote the data from different specimens.

Moreover, the present results for the VHCF behavior of the bearing steel specimens show that the grain refinement only exists in some regions beneath FGA. This indicates that the micro cracks might initiate along the boundaries of refined and common grains [22], or initiate at the interior of the common grains or the grain boundaries etc (i.e. irrespective of the grain refinement) [34–36] due to the microstructure inhomogeneities or the high strain localization [37].

Therefore, it is thought that the mechanism of the crack initiation and early growth for high strength steels in VHCF regime is attributed to the formation of grain refinement caused by the dislocation interaction over a number of cyclic loadings followed by micro cracks and the formation of the micro cracks irrespective of the grain refinement as proposed by Sun et al. [22], which could be further described as follows, and shown in Fig. 9.

**Stage I**: The high strain localization induced by defects or microstructural inhomogeneities leads to the irreversible plastic deformation accumulation followed by the small crack nuclei at the inclusion, the interface of matrix and inclusion, the grain or grain boundaries, etc. During the crack nuclei process, the cyclic loading might also induce the formation of dislocation or dislocation cell in some local regions.

**Stage II**: Grain refinement is caused by the microstructure evolution with the help of the dislocation interaction over a number of cyclic loadings. Then, the micro cracks form within the refined grains or along the boundaries of the refined grain and the common grain. Meanwhile, the formation of micro cracks might occur irrespective of the grain refinement under the cycling loadings, which results in no grain refinement characteristic beneath the crack surface in some regions.

**Stage III**: The micro cracks coalesce during the further cyclic loadings. Meanwhile, some new micro cracks form or grain refinement happens followed by the formation of micro cracks. The main crack extends and forms parts of the crack initiation and early growth region (FGA). The increased stress concentration due to the growing crack initiation and early growth region causes the grain refinement or formation of micro cracks again (i.e. Stage II).

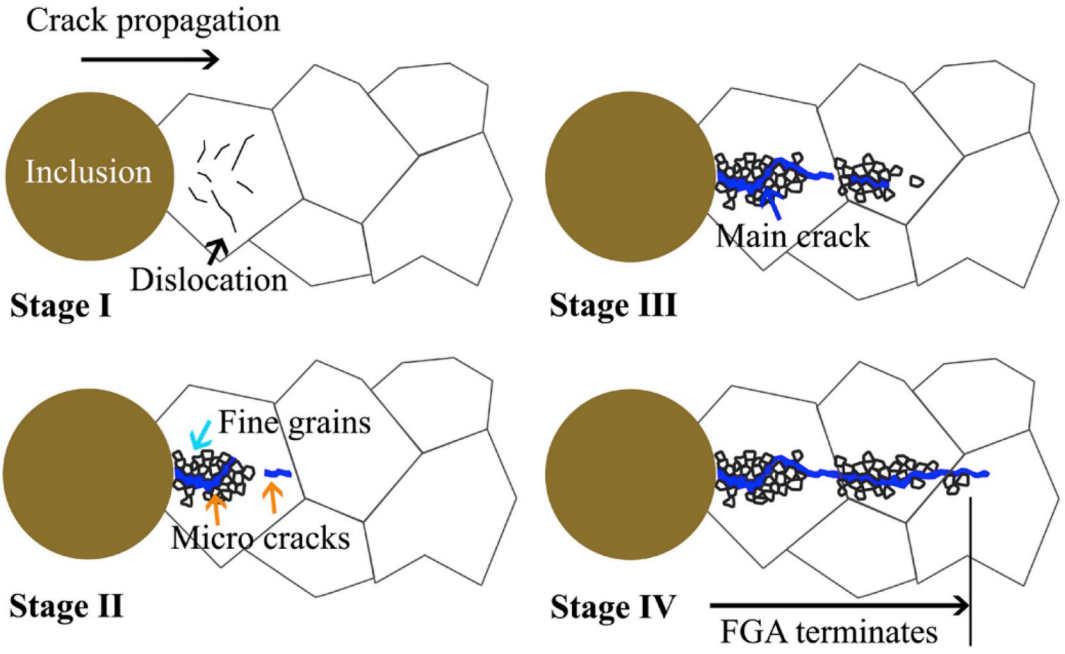


**Fig. 9.** Sketch map of the mechanism of crack initiation and early growth for high strength steels in VHCF regime.

**Stage IV**: The process of grain refinement or micro crack formation continues, and then coalesces under the further fatigue loading until the crack initiation and early growth region (FGA) reaches the critical size, which might be determined by the threshold value of the crack propagation.

It is noted that the crack could initiate at the inclusion, the interface of matrix and inclusion, the grain or grain boundaries etc [16,35], as shown in Figs. 3 and 5. Also, the FGA (rough area) morphology or grain refinement might not present in the crack initiation and early growth region for VHCF of high strength steels in some cases [19,28,29]. The sketch map in Fig. 9 just presents the case of crack initiation from the inclusion with FGA morphology and discontinuous refined grain regions for VHCF of high strength steels. Additionally, due to that the stress intensity factor range at the front of FGA is close to the threshold value of crack propagation $\Delta K_{th}$ [15–17], the grain refinement should usually occur in the grains not far from the crack initiation site and the number of grains that the grain refinement appears depends on the stress level and the grain size of the material.

## 5. Conclusions

The mechanism of the crack initiation and early growth of high strength steels in VHCF regime is investigated by specially designed variable amplitude loadings and compressive fatigue test. The main results are summarized as follows:

(1) Discontinuous refined grain regions are observed beneath the fracture surface in the crack initiation and early growth region (FGA) for the bearing steel with tensile strength bigger than 2000 MPa in VHCF regime. The grain refinement phenomenon is not observed in the vicinity of the crack tip and in the region beneath the crack surface after $5 \times 10^6$ cyclic compressive loadings for the martensitic stainless steel specimen with a pre-crack, indicating that the grain refinement is formed during the crack initiation and evolution process.

(2) The traces left on the fracture surface by the variable amplitude loadings show that the equivalent crack growth length in the crack initiation and early growth stage (FGA) per cycle is much lower than one lattice spacing ($\sim 10^{-10}$ m). A condition is proposed for the critical size of FGA from the view of crack propagation rate, namely, that the FGA developing is completed when the stress intensity factor range of FGA reaches to the threshold value of the crack propagation $\Delta K_{th}$.

(3) The paper suggests that the crack initiation and early growth of high strength steels is attributed to the grain refinement caused by the dislocation interaction over a number of cyclic loadings followed by micro cracks along with the formation of the micro cracks at the interior of the common grains or the grain boundaries etc (i.e. irrespective of grain refinement) during the cyclic loading. This model could explain the experimental phenomena that the microstructure beneath the crack initiation and early growth region could be a thin layer of nanograins, discontinuous refined grain regions and no refined grain feature in VHCF regime.

## Declaration of competing interest

The authors declare that they have no known competing financial interests or personal relationships that could have appeared to influence the work reported in this paper.

## Acknowledgements

The authors gratefully acknowledge the support of the National Key R&D Program of China (2017YFA0204402), the National Natural Science Foundation of China (91860112) and the Strategic Priority Research Program of the Chinese Academy of Sciences (XDB22020200).

## References

[1] S. Gupta, A. Barrios, No England, O.N. Pierron, Improved very high cycle bending fatigue behavior of Ni microbeams with Au coatings, Acta Mater. 161 (2018) 444–455.
[2] M.L. Zhu, L. Jin, F.Z. Xuan, Fatigue life and mechanistic modeling of interior micro-defect induced cracking in high cycle and very high cycle regimes, Acta Mater. 157 (2018) 259–275.
[3] C. Sun, Q. Song, Y. Hu, Y. Wei, Effects of intermittent loading on fatigue life of a high strength steel in very high cycle fatigue regime, Int. J. Fatigue 117 (2018) 9–12.
[4] Y. Murakami, T. Nomoto, T. Ueda, Factors influencing the mechanism of superlong fatigue failure in steels, Fatigue Fract. Eng. Mater. Struct. 22 (1999) 581–590.
[5] Z. Huang, D. Wagner, C. Bathias, P.C. Paris, Subsurface crack initiation and propagation mechanisms in gigacycle fatigue, Acta Mater. 58 (2010) 6046–6054.
[6] X.G. Wang, E.S. Feng, C. Jiang, A microplasticity evaluation method in very high cycle fatigue, Int. J. Fatigue 94 (2017) 6–15.
[7] T. Sakai, Y. Sato, Y. Nagano, M. Takeda, N. Oguma, Effect of stress ratio on long life fatigue behavior of high carbon chromium bearing steel under axial loading, Int. J. Fatigue 28 (2006) 1547–1554.
[8] K. Shiozawa, T. Hasegawa, Y. Kashiwagi, L. Lu, Very high cycle fatigue properties of bearing steel under axial loading condition, Int. J. Fatigue 31 (2009) 880–888.
[9] C. Sun, Z. Lei, J. Xie, Y. Hong, Effects of inclusion size and stress ratio on fatigue strength for high-strength steels with fish-eye mode failure, Int. J. Fatigue 48 (2013) 19–27.
[10] H. Abdesselam, J. Crepin, A. Pineau, A.L. Rouffie, P. Gaborit, L. Menut-Tournadre, T.F. Morgeneyer, On the crystallographic, stage I-like, character of fine granular area formation in internal fish-eye fatigue cracks, Int. J. Fatigue 106 (2018) 132–142.
[11] X. Liu, E. Chen, F. Zeng, T. Cong, J.P. Domblesky, Mechanisms of interior crack initiation in very-high-cycle fatigue of high-strength alloys, Eng. Fract. Mech. 212 (2019) 153–163.
[12] K. Shiozawa, Y. Morii, S. Nishino, L. Lu, Subsurface crack initiation and propagation mechanism in high strength steel in a very high cycle fatigue regime, Int. J. Fatigue 28 (2006) 1521–1532.
[13] Q.Y. Wang, C. Bathias, N. Kawagoishi, Q. Chen, Effect of inclusion on subsurface crack initiation and gigacycle fatigue strength, Int. J. Fatigue 24 (2002) 1269–1274.
[14] Y. Hong, Z. Lei, C. Sun, A. Zhao, Propensities of crack interior initiation and early growth for very-high-cycle fatigue of high strength steels, Int. J. Fatigue 58 (2014) 144–151.
[15] T. Sakai, Review and prospects for current studies on very high cycle fatigue of metallic materials for machine structural use, J. Solid Mech. Mater. Eng. 3 (2009) 425–439.
[16] A. Zhao, J. Xie, C. Sun, Z. Lei, Y. Hong, Prediction of threshold value for FGA formation, Mater. Sci. Eng. A 528 (2011) 872–877.
[17] C. Sun, X. Liu, Y. Hong, A two-parameter model to predict fatigue life of high-strength steels in a very high cycle fatigue regime, Acta Mech. Sin. 31 (2015) 383–391.
[18] P. Grad, B. Reuscher, A. Brodyanski, Mechanism of fatigue crack initiation and propagation in the very high cycle fatigue regime of high-strength steels, Scr. Mater. 67 (2012) 838–841.
[19] Y. Hong, X. Liu, Z. Lei, C. Sun, The formation mechanism of characteristic region at crack initiation for very-high-cycle fatigue of high-strength steels, Int. J. Fatigue 89 (2016) 108–118.
[20] D. Spriestersbach, A. Brodyanski, J. Lösch, M. Kopnarski, E. Kerscher, Very high cycle fatigue of bearing steels with artificial defects, Proc. Struct. Integr. 2 (2016) 1101–1108.
[21] M.W. Tofique, J. Bergström, K. Svensson, Very high cycle fatigue of cold rolled stainless steels, crack initiation and formation of the fine granular area, Int. J. Fatigue 100 (2017) 238–250.
[22] C. Sun, Q. Song, L. Zhou, J. Liu, Y. Wang, X. Wu, Y. Wei, The formation of discontinuous gradient regimes during crack initiation in high strength steels under very high cycle fatigue, Int. J. Fatigue 124 (2019) 483–492.
[23] T. Sakai, N. Oguma, A. Morikawa, Microscopic and nanoscopic observations of metallurgical structures around inclusions at interior crack initiation site for a bearing steel in very high-cycle fatigue, Fatigue Fract. Eng. Mater. Struct. 38 (2015) 1305–1314.
[24] S. Kovacs, T. Beck, L. Singheiser, Influence of mean stresses on fatigue life and damage of a turbine blade steel in the VHCF-regime, Int. J. Fatigue 49 (2013) 90–99.
[25] Y. Murakami, T. Nomoto, T. Ueda, On the mechanism of fatigue failure in the superlong life regime (N>107 cycles). Part I: influence of hydrogen trapped by inclusions, Fatigue Fract. Eng. Mater. Struct. 23 (2000) 893–902.
[26] T. Nakamura, H. Oguma, Y. Shinohara, The effect of vacuum-like environment inside sub-surface fatigue crack on the formation of ODA fracture surface in high strength steel, Procedia Eng. 2 (2010) 2121–2129.
[27] D. Spriestersbach, P. Grad, A. Brodyanski, J. Lösch, M. Kopnarski, E. Kerscher, Very high cycle fatigue crack initiation: investigation of fatigue mechanisms and threshold values for 100Cr6, in: H.-J. Christ (Ed.), Fatigue of Materials at Very High Numbers of Loading Cycles, 2018, pp. 167–210.

[28] G. Qian, C. Zhou, Y. Hong, Experimental and theoretical investigation of environmental media on very-high-cycle fatigue behavior for a structural steel, Acta Mater. 59 (2011) 1321–1327.
[29] M. Sander, T. Müller, J. Lebahn, Influence of mean stress and variable amplitude loading on the fatigue behaviour of a high-strength steel in VHCF regime, Int. J. Fatigue 62 (2014) 10–20.
[30] C. Sun, Q. Song, L. Zhou, X. Pan, Characteristic of interior crack initiation and early growth for high cycle and very high cycle fatigue of a martensitic stainless steel, Mater. Sci. Eng. A 758 (2019) 112–120.
[31] S. Suresh, Fatigue of Materials, in: Z.G. Wang, et al. (Eds.), Trans. In Chinese, second ed., National Defense Industry Press, Beijing, 1999, p. 436.
[32] Z. Yang, S. Li, Y. Liu, G. Li, W. Hui, Y. Weng, Estimation of the size of GBF area on fracture surface for high strength steels in very high cycle fatigue regime, Int. J. Fatigue 30 (2008) 1016–1023.
[33] I. Marines-Garcia, P.C. Paris, H. Tada, C. Bathias, D. Lados, Fatigue crack growth from small to large cracks on very high cycle fatigue with fish-eye failures, Eng. Fract. Mech. 75 (2008) 1657–1665.
[34] J. Bach, J.J. Möller, M. Göken, E. Bitzek, H.W. Höppel, On the transition from plastic deformation to crack initiation in the high- and very high-cycle fatigue regimes in plain carbon steels, Int. J. Fatigue 93 (2016) 281–291.
[35] Q. Jiang, C. Sun, X. Liu, Y. Hong, Very-high-cycle fatigue behavior of a structural steel with and without induced surface defects, Int. J. Fatigue 93 (2016) 352–362.
[36] N. Torabian, V. Favier, J. Dirrenberger, F. Adamski, S. Ziaei-Rad, N. Ranc, Correlation of the high and very high cycle fatigue response of ferrite based steels with strain rate-temperature conditions, Acta Mater. 134 (2017) 40–52.
[37] G. Chai, N. Zhou, S. Ciurea, M. Andersson, R.L. Peng, Local plasticity exhaustion in a very high cycle fatigue regime, Scr. Mater. 66 (2012) 769–772.